Free-stream coherent structures in the unsteady Rayleigh boundary layer

DOI:
10.1093/imamat/hxaa038

Document Version
Accepted author manuscript

IMA Journal of Applied Mathematics (2020) Page 1 of 20
doi:10.1093/imamat/iarxxx

Free-stream coherent structures in the unsteady Rayleigh boundary layer

ELEANOR C. JOHNSTONE*
School of Mathematics, University of Manchester, Manchester M13 9PL, UK
*Corresponding author: eleanor.johnstone@manchester.ac.uk

AND

PHILIP HALL
School of Mathematics, Monash University, Melbourne, VIC 3800, Australia

[Received on XX XX XXXX; revised on XX XX XXXX; accepted on XX XX XXXX]

Results are presented for nonlinear equilibrium solutions of the Navier–Stokes equations in the boundary layer set up by a flat plate started impulsively from rest. The solutions take the form of a wave–roll–streak interaction which takes place in a layer located at the edge of the boundary layer. This extends previous results for similar nonlinear equilibrium solutions in steady two-dimensional boundary layers. The results are derived asymptotically and then compared to numerical results obtained by marching the reduced boundary-region disturbance equations forward in time. It is concluded that the previously found canonical free-stream coherent structures in steady boundary layers can be embedded in unbounded, unsteady shear flows.

Keywords: transition to turbulence, unsteady transition, boundary layer stability

1. Introduction

There are fundamental differences in the instability and transition processes in steady and unsteady flows. The asymptotic description of nonlinear equilibrium solutions of the Navier–Stokes equations, which has been suggested gives an insight into transition in shear flows, has previously only been conducted in the context of steady flows. We present results for nonlinear equilibrium solutions in the unsteady boundary layer set up by a flat plate moved impulsively from rest, hereafter referred to as the Rayleigh problem.

The solutions we are interested in are equilibrium solutions of the Navier–Stokes equations as fixed points or periodic orbits for shear flows. Their underlying physics is very similar to that described by vortex-wave interaction (VWI) theory (Hall & Smith, 1991): a streak is unstable to a three-dimensional wave which interacts with itself in a critical layer to produce a roll via Reynolds stresses. This roll then drives the streak, resulting in a 'self-sustaining process' (Waleffe, 1997). These types of solutions, often referred to as 'exact coherent structures', have been found both numerically and asymptotically in the high Reynolds number limit for a range of steady flows (see, for example, Faisst & Eckhardt 2003; Waleffe 2001, 2003; Wedin & Kerswell 2004; Wang et al. 2007, Hall & Sherwin 2010, Deguchi & Hall 2014a).

However, the solutions discussed here differ from the exact coherent structures because the roll-streak interaction takes place in a layer which sits just below the free-stream; this layer is termed the 'production layer' by Deguchi & Hall (2014b), who first observed these 'free-stream coherent structures' in parallel asymptotic suction boundary layer (ASBL) flow, and replaces the traditional critical layer in

VWI theory which sits in the boundary layer.

Deguchi & Hall (2014b) solve the full Navier–Stokes equations within the production layer as a nonlinear eigenvalue problem of unit Reynolds number; this solution then motivates an asymptotic description of the flow above and below the layer. Above the layer all disturbances decay, whilst below the layer the interaction of the perturbation with the background flow produces a streak disturbance which grows exponentially below the layer via a nonlinear interaction between the roll and the mean flow, before obtaining its maximum size in the near-wall boundary layer. The existence of the structures relies upon the fact that the background state is of boundary-layer form, and that in the production layer the difference between the streamwise velocity and the free-stream speed is exponentially small, which allows the nonlinear interaction to take place. The key implication is that streak disturbances seen at the wall could have their origin much further away.

Free-stream coherent structures have since been described in a wide range of general steady shear flows such as the Burger's vortex sheet (Deguchi & Hall, 2014a); spatially-growing two dimensional boundary layers such as Blasius flow (Deguchi & Hall, 2015); and planar jets (Deguchi & Hall, 2018). The asymptotic description of free-stream coherent structures in the Rayleigh problem is very similar to those described by (Deguchi & Hall, 2015) for spatially-growing two-dimensional boundary layers which approach their free-stream form exponentially. They show that the production layer problem for these flows can, remarkably, be reduced to exactly that of the ASBL flow, albeit with local values of the wavenumbers. However below the production layer non-parallel effects came into play to give a rich asymptotic structure comprising of two 'adjustment layers' and an irrotational layer connected by diffusion fronts. These curves arise due to the coalescing of different Wentzel–Kramers–Brillouin (WKB) phases. As in the ASBL problem, the streak disturbance grows exponentially beneath the production layer towards the wall but this time obtains its maximum in the lower adjustment layer where the WKB amplitude is a minimum. The asymptotic results for large Reynolds number agree well with numerical solutions of the parabolic boundary-region equations for the disturbance.

We now describe free-stream coherent structures in the unsteady boundary layer arising from a flat plate set in impulsive motion from rest. The importance of unsteady effects on the stability of time-dependent flows has been studied for a wide range of problems, including an impulsively-started rotating cylinder Chen & Christensen (1967); time-dependent rotational Couette flow (Kirchner & Chen, 1970); and the flow around a cylinder immersed in fluid which is impulsively spun up (Otto, 1993). Of particular interest is the reconciliation of the onset of transition in unsteady flows with predictions of instability from linear stability analysis; Moss (1992) show that for impulsively-started pipe flow the onset of transition occurs at lower Reynolds numbers than linear predictions of instability. The effect of unsteadiness on the onset of transition and instability is attributed to an upstream travelling turbulent front leading to finite-amplitude disturbances.

Even for slowly-varying flows which can be studied using a quasi-static approach, the stabilising effect of the quasi-static assumption is often not enough to overcome instabilities arising from the time-dependent nature of the flow (Shen, 1961; Von Kerczek & Davis, 1974; Seminara & Hall, 1975). Unsteady effects have been shown to be particularly important in the linear stability of Stokes problem (an impulsively-started flat plate in oscillatory motion) which is governed by unstable Floquet modes (and non-Floquet modes appear at high Reynolds numbers) (Von Kerczek & Davis, 1974; Hall, 1978; Cowley, 1987; Hall, 2003); when unsteady effects are amplified, such as a skewed acceleration of the plate, the problem becomes linearly unstable at lower Reynolds number (Thomas, 2020). Unsteadiness also changes the nature of the route to turbulence for the Stokes problem through the presence of a finite-time singularity and the growth of three-dimensional disturbances interacting with two-dimensional

waves using a critical layer approach (Wu 1992; Wu et al. 1993). In fact, Wu et al. (1993) link the unsteady critical-layer approach and the vortex-wave interaction theory of Hall & Smith (1991) in the context of a linear disturbance evolving to an unsteady critical-layer type interaction, and then further evolving into a VWI-type state. It has been suggested that these VWI states, *i.e.* the exact and free-stream coherent structures described above, are a key building block of shear-flow transition processes; for a more complete discussion of this suggestion the reader is referred to Jiménez (2018) and the introduction of Deguchi & Hall (2015). Therefore, a key implication of the problem discussed in this paper is that there may be a connection between transition in steady and unsteady flows.

The unsteady boundary-region equations which appear in this paper are also discussed by Ricco et al. (2011) where they are found to govern the evolution of streaky boundary-layer disturbances from unsteady free-stream turbulence. Unlike the case for steady disturbances, streaky boundary layers generated by unstable disturbances are inviscidly unstable and thus boundary layer transition can occur without separation (Goldstein & Sescu, 2008). The unsteady boundary-region equations considered in this paper are reduced, through a suitable transformation, to the well-known Görtler vortex equations of Hall (1983) with unit Görtler number; these also appear as the governing equations for three-dimensional boundary-layer perturbations in the problem studied by Luchini (1996). Their numerical solution is discussed thoroughly by Hall (1983); for extensive numerical studies of more complex nonlinear boundary-region equations the reader is referred to Martin & Martel (2012) and Sescu & Afsar (2018).

Little is known about the stability of fluid flows with a general time dependence; the meaning of stability is not clear when the magnitude of the basic flow changes over time. That being said, using the assumptions of Hall & Parker (1976) and Cowley (1987) that quasi-steady flow is justified at high Reynolds number with a fast convective time scale, then Rayleigh flow may be considered quasi-steady; indeed the time dependence of the free-stream coherent structure problem is absorbed in the similarity variable so that instantaneously the flow sees the disturbance as steady. Under this assumption it could be suggested that there exists a similar mechanism for the transition process in steady and quasi-steady flows.

In this paper we apply the approach of Deguchi & Hall (2015) for spatially-growing boundary layers to Rayleigh's problem. The study of the unsteady problem is motivated by the Gaussian approach of the unperturbed flow to its free-stream form. Deguchi & Hall (2014b) show that for the ASBL problem this approach actually needs to be an exponential function of distance from the wall. We show that the unsteadiness in the Rayleigh problem can mimic the suction of ASBL flow to force the flow to instantaneously decay with the required exponential behaviour using a scaled variable.

We see that through an appropriate transformation the production-layer problem can be reduced to exactly the 'parallel' problem of ASBL flow through the introduction of a similarity variable which captures the time-dependence of the problem. However, as with the spatially-developing case, below the layer unsteady effects come back into play and the problem has to be considered instantaneously at each time step, with instantaneous values of the frequency and wavenumbers. This gives rise to a complex asymptotic structure due to the changing dominance of the different WKB solutions, however it also means that full numerical simulations would be very computationally demanding. This is not necessary however, as the results of the locally parallel nonlinear eigenvalue problem of Deguchi & Hall (2014b) can be used to determine the instantaneous wavenumbers at each time step, thereby allowing the parabolic boundary-region equations to be marched forward in time to give a comparison to the analytical results.

The procedure adopted for the rest of this paper is as follows: in §2 we outline the problem for

Rayleigh flow before the production layer problem is derived in §3 and the flow beneath the production layer is described in §4. In §5 numerical results are computed. In §6 a general discussion of our results in the context of existing research is given, as well as comments on further questions to be explored.

2. The basic flow for the Rayleigh problem

Consider a viscous flow with viscosity ν above an infinitely long flat plate at $y^* = 0$ with respect to Cartesian co-ordinates (x^*, y^*, z^*). At time $t^* = 0$, the plate is impulsively set into motion and continues moving with constant velocity $-U_1$, where the sign is chosen to allow an easier comparison to the Deguchi & Hall (2014b) ASBL problem. Therefore, if the velocity of the flow is $\boldsymbol{u}^* = (u^*, v^*, w^*)$, then the boundary conditions are $\boldsymbol{u}^* \to (0,0,0)$ a long way from the plate, and $\boldsymbol{u}^* = (-U_1, 0, 0)$ at the plate.

Taking τ as a typical time-scale for the development of the flow, the width of the boundary layer that forms on the plate surface is found to be $\sqrt{\nu\tau}$. If we non-dimensionalize using this length scale and U_1 as a typical flow speed, the Reynolds number of the problem is found to be $Re = U_1\sqrt{\tau/\nu}$. Then, the equations of motion describing the non-dimensional flow field are

$$\frac{1}{Re}\boldsymbol{u}_t + (\boldsymbol{u}\cdot\boldsymbol{\nabla})\boldsymbol{u} = -\boldsymbol{\nabla}p + \frac{1}{Re}\nabla^2\boldsymbol{u}, \tag{2.1}$$

$$\boldsymbol{\nabla}\cdot\boldsymbol{u} = 0. \tag{2.2}$$

For the Rayleigh problem, the flow is uniform in the x-direction as the plate is moving with constant speed and there is no velocity in the spanwise direction. Hence, the flow is transient but only changes in the y-direction. Under these assumptions, the high-Reynolds-number equations of motion reduce to $u_t = u_{yy}$, where subscript represents partial derivative. This equation can be solved via the introduction of a similarity variable $\eta = y(2t)^{-1/2}$, where the scaling is chosen for convenience, so that we seek solutions in the form $u = \bar{u}(\eta)$. Thus, we solve

$$\bar{u}'' + \eta\bar{u}' = 0, \quad \bar{u}(0) = -1, \quad \bar{u}(\infty) = 0, \tag{2.3a–c}$$

where prime denotes derivative, to find that

$$\bar{u} = \mathrm{erf}(\eta/2) - 1. \tag{2.4}$$

Therefore at large values of η, i.e. as the free-stream is approached, the streamwise velocity is given by

$$u(t,y) \approx -A_0\eta^{-1}\mathrm{e}^{-\eta^2/2} = -A_0 y^{-1}\sqrt{2t}\,\mathrm{e}^{-y^2/4t}, \tag{2.5}$$

where $A_0 = \sqrt{2/\pi}$.

3. The production layer problem

If the Reynolds number is large, the equations of motion allow for other solutions including the free-stream coherent structures described in Deguchi & Hall (2014b). The production layer, where the nonlinear interaction that produces the structures takes place, is completely distinguished from the near-wall boundary layer. In this layer waves, rolls and streaks interact in a self-sustaining manner to produce a coherent structure that is convected downstream with almost the free-stream speed. The interaction of the roll flow and the mean flow enables the streak disturbance to grow exponentially beneath the layer.

3.1 *Free-stream coherent structures in parallel boundary-layer flows*

We will show that we are able to reduce the production-later problem for the unsteady Rayleigh flow to the production layer problem for parallel ASBL flow. Therefore in order to give some context to the results for free-stream coherent structures in the Rayleigh problem, we shall very briefly summarize the results of Deguchi & Hall (2014b) for the canonical parallel ASBL problem. These were described completely in that paper and summarised in Deguchi & Hall (2015), therefore only a brief description shall be given here.

ASBL flow is a viscous flow over an infinitely long flat plate; the basic flow is therefore independent of x and z with respect to Cartesian co-ordinates (x,y,z). The plate has small perforations where a low pressure gradient is maintained so the fluid is sucked downwards through the plate at constant velocity. The suction forces a parallel boundary layer on the plate surface. The basic flow is given by

$$\boldsymbol{u}_b = (u_b, -Re^{-1}, 0) = (1-\mathrm{e}^{-y}, -Re^{-1}, 0), \tag{3.1}$$

with the Reynolds number Re based on the free-stream speed and the unperturbed boundary-layer thickness. If we perturb the flow at high Reynolds numbers we find a nonlinear interaction taking place in a layer located at $Y = y - \ln Re$. This layer is situated just below the free-stream and the structure created is convected downstream with speed differing from the free-stream speed by $O(Re^{-1})$ so that the wave dependence in the layer is defined as $X = x - ct$, $c = 1 - Re^{-1}c_1 + \cdots$. The equations describing the interaction form a nonlinear eigenvalue problem at unit Reynolds number for the wavespeed c_1 and are given by

$$([\boldsymbol{U} + c_1\hat{\boldsymbol{i}}]\cdot\boldsymbol{\nabla})\boldsymbol{U} = -\boldsymbol{\nabla}P + \nabla^2\boldsymbol{U}; \quad \boldsymbol{\nabla}\cdot\boldsymbol{U} = 0, \tag{3.2a,b}$$

where $\boldsymbol{U} = (U,V,W)$ and P are the perturbation velocity and pressure scaled on Re^{-1} and Re^{-2} respectively. This is then a nonlinear eigenvalue problem for the wavespeed c_1. This system is to be solved subject to boundary and periodicity conditions given by

$$\boldsymbol{U} \to (0,-1,0) \text{ as } Y \to \infty; \quad \boldsymbol{U} \to (-\mathrm{e}^{-Y}, -1, 0) \text{ as } Y \to -\infty,$$

$$\boldsymbol{U}(X,Y,Z) = \boldsymbol{U}(X + 2\pi/\alpha, Y, Z), \quad \boldsymbol{U}(X,Y,Z) = \boldsymbol{U}(X,Y,Z+2\pi/\beta). \tag{3.3a-d}$$

Here, α and β are the streamwise and spanwise wavenumbers respectively. The key point to notice here is that the second of these boundary conditions (3.3b) allows for the possibility of higher-order X-independent terms of U to grow exponentially beneath the production layer, although the growth would be at a slower rate than the leading order growth $\sim e^{-Y}$.

Below the layer the disturbance field adjusts to become compatible with the basic flow, therefore this layer is termed the 'adjustment layer'. In order to analyse the growth of the higher-order terms in the adjustment layer, the flow is split into its mean flow, vortex and wave components. The mean flow is the average in X and Z of the flow, whilst the vortex component is the average in X of the disturbance only. The streak is the vortex component of U and the roll is the vortex component of (V,W). The equations for the leading order vortex components are then Fourier analysed to yield the form of the solution beneath the production layer:

$$U \to -\mathrm{e}^{-Y} + J_1\mathrm{e}^{(\omega_1-1)Y}\cos(2\beta Z) + \ldots; \quad V \to -1 + K_1\mathrm{e}^{\omega_1 Y}\cos(2\beta Z) + \ldots, \tag{3.4a,b}$$

where $K_1 = K_1(\alpha,\beta)$ is to be found as part of the numerical eigenvalue problem in the production layer and

$$\omega_1 = (\sqrt{1+16\beta^2} - 1)/2 > 0, \quad J_1 = -K_1/2\omega_1. \tag{3.5a,b}$$

Hence, we see that exponential growth of the streak only occurs for spanwise wavenumbers in the range $\beta < 1/\sqrt{2}$. It is found that as the wall is approached, where all disturbances must ultimately be reduced to zero, the streak disturbance takes its maximum within the unperturbed near-wall boundary layer. Thus the crucial conclusion is that a nonlinear interaction in the free-stream involving a velocity field of size $O(Re^{-1})$ can produce a much larger streak disturbance which is felt most strongly in the boundary layer, away from the production layer where it is generated. It should be noted that the wave and roll field decay below the production layer as the self-sustaining mechanism, which provides the forcing to the roll flow via the Reynolds stresses associated with the wave, is localized in the production layer. Numerical results at finite Reynolds number shown in Deguchi & Hall (2014b) agree well with the asymptotic theory shown above.

3.2 *The production layer problem for Rayleigh flow*

The free-stream coherent structures in ASBL flow described in §3.1 owe their existence to the fact that the basic flow approaches its free-stream form through an exponential function of distance from the wall. Deguchi & Hall (2015) show that an arbitrary two-dimensional spatially-developing boundary layer, which instead approaches its free-stream form via an exponential function of the square of distance from the wall (Brown & Stewartson, 1965), can also support the structures through an appropriate transformation which forces the decay to be of the required form locally around the production layer. This effect of boundary-layer growth is crucial to the interaction mimicking the ASBL structure in the production layer. We shall see that the same holds true of the Rayleigh problem, but with unsteady effects replacing the effect of boundary layer growth.

We first find the location and scalings required to define the nonlinear eigenvalue problem to be solved in the production layer for the Rayleigh problem, and then show how this can be transformed into the canonical production-layer problem (3.2)–(3.3) in §3.1.

3.3 *Location and scalings*

We seek a structure which is periodic in the streamwise and spanwise directions, with wavenumbers α_0 and β_0 respectively. It is located in a layer of unknown thickness δ_p situated at an unknown distance K from the wall; the layer is situated just below the free-stream so $K \gg 1$. Writing $y(2t)^{-1/2} = K + \delta_p \tilde{Y}(2t)^{-1/2}$, we see that for large K, in order for the flow to decay locally as a function of exponential distance from the wall we must take $\delta_p = K^{-1}$. In this case,

$$u \approx -A_0 K^{-1} \mathrm{e}^{-K^2/2} \mathrm{e}^{-\tilde{Y}/\sqrt{2t}}. \tag{3.6}$$

We now fix K by considering a balance of terms in the streamwise momentum equation. Previous work by Deguchi & Hall 2014b, 2015 has shown that the free-stream coherent structures in the production layer are nonlinear wave structures with wavelengths comparable to the boundary layer scale. Therefore, with respect to the scaling for y in the production layer and the boundary-layer scalings in §2, the structure will operate in a cube of sides length $\delta_p = K^{-1}$ within the viscous production layer. The nonlinear terms and viscous terms will thus balance if

$$\frac{1}{K} \exp\left[\frac{-K^2}{2}\right] = \frac{K^2}{Re} \qquad \Rightarrow K \approx \sqrt{2 \ln Re}. \tag{3.7}$$

We now restrict any streamwise dependence to be in the form of a wave moving downstream with almost the free-stream speed; because the boundary-layer is growing in time, the wavespeed must also change

in time. If the streamwise wavelength is also to remain comparable with the depth of the layer and the convective balance $\partial_t + u\partial_x \sim O(K^2/Re)$ is to be maintained, then in the production layer we write

$$\tilde{\Phi} = K\alpha_0\left[x - K\int^t c(\tilde{t})\,\mathrm{d}\tilde{t}\right], \quad \frac{y}{\sqrt{2t}} = K + \frac{\tilde{Y}}{K\sqrt{2t}}, \quad \tilde{Z} = Kz. \tag{3.8a-c}$$

Here α_0 is the streamwise wavenumber, which is constant because the base flow of Rayleigh problem is not spatially dependent. Therefore, unlike the growing boundary layer problem studied in Deguchi & Hall (2015), where local streamwise wavenumbers $\alpha_0(x)$ were defined in terms of the (non-zero) free-stream speed $U_1(x)$, there are no difficulties if the free-stream speed is zero. We also note that if $c(t)$ is constant then the phase variable $\tilde{\Phi}$ reduces to the wave dependence seen in ASBL flow in §3.1. The scalings for the velocity field can be found by considering the continuity equation (2.2). We find $u \sim v \sim w \sim O(KRe^{-1})$, then the pressure must be $O(K^2Re^{-2})$ to be kept in play, so we seek a solution in the form

$$\boldsymbol{u} = KRe^{-1}\tilde{\boldsymbol{U}}(t,\tilde{\Phi},\tilde{Y},\tilde{Z}), \qquad p = K^2Re^{-2}\tilde{P}(t,\tilde{\Phi},\tilde{Y},\tilde{Z}). \tag{3.9a,b}$$

We substitute this expansion into the equations of motion (2.1) and (2.2) to find the nonlinear eigenvalue problem for the instantaneous wavespeed to be solved in the production layer:

$$\left[\left(\tilde{\boldsymbol{U}} - c(t)\hat{\boldsymbol{i}} - \frac{1}{\sqrt{2t}}\hat{\boldsymbol{j}}\right)\cdot\tilde{\boldsymbol{\nabla}}\right]\tilde{\boldsymbol{U}} = -\tilde{\boldsymbol{\nabla}}\tilde{P} + \tilde{\nabla}^2\tilde{\boldsymbol{U}}, \tag{3.10}$$

$$\tilde{\boldsymbol{\nabla}}\cdot\tilde{\boldsymbol{U}} = 0, \tag{3.11}$$

where $\tilde{\boldsymbol{\nabla}} = (\alpha_0\partial_{\tilde{\Phi}}, \partial_{\tilde{Y}}, \partial_{\tilde{Z}})$ and $\tilde{\nabla}^2 = \alpha_0^2\partial_{\tilde{\Phi}}^2 + \partial_{\tilde{Y}}^2 + \partial_{\tilde{Z}}^2$, and the equations are to be solved subject to boundary conditions

$$\tilde{U} \to 0 \quad \text{as} \quad \tilde{Y} \to \infty, \tag{3.12a}$$

$$\tilde{U} \to -A_0\mathrm{e}^{-\tilde{Y}/\sqrt{2t}} \quad \text{as} \quad \tilde{Y} \to -\infty, \tag{3.12b}$$

and periodicity conditions

$$(\tilde{\boldsymbol{U}},\tilde{P})(t,\tilde{\Phi},\tilde{Y},\tilde{Z}+2\pi/\beta_0) = \boldsymbol{U}(t,\tilde{\Phi},\tilde{Y},\tilde{Z}), \tag{3.13a}$$

$$(\tilde{\boldsymbol{U}},\tilde{P})(t,\tilde{\Phi}+2\pi,\tilde{Y},\tilde{Z}) = \boldsymbol{U}(t,\tilde{\Phi},\tilde{Y},\tilde{Z}), \tag{3.13b}$$

where β_0 is the spanwise wavenumber. It is of crucial importance to notice the $(2t)^{-1/2}\partial_{\tilde{Y}}$ term in the momentum equation (3.10); this represents a 'suction-like' effect which has been produced by unsteady effects in the boundary layer. The portion of the flow travelling closest to the wall is subject to this suction-like effect which serves to thicken the velocity profile. The effect here gets weaker as time increases, and hence forces the production-layer flow to be quasi-steady.

3.4 *Reduction to the ASBL production layer problem*

The problem above looks similar to the nonlinear eigenvalue problem (3.2)–(3.3) described in §3.1 for ASBL flow. Indeed, if we consider the transformation

$$\tilde{\Phi} = \alpha_0\sqrt{2t}\Phi, \quad \tilde{Y} = \sqrt{2t}\left[Y + \ln(A_0\sqrt{2t})\right], \quad \tilde{Z} = \sqrt{2t}Z, \quad c = -c_1/\sqrt{2t}$$

$$(\tilde{U},\tilde{V},\tilde{W},\tilde{P}) = (\sqrt{2t})^{-1}(U,V+1,W,P), \qquad (3.14a-e)$$

then (3.10)–(3.13) become exactly the ASBL nonlinear eigenvalue problem (3.2)–(3.3) but with time-dependent values of the effective wavenumbers $\alpha = \alpha_0\sqrt{2t}$ and $\beta = \beta_0\sqrt{2t}$ (we note that the wavenumbers for the Rayleigh problem are constant). This means that at each timestep, solutions of the Rayleigh problem can be extracted by using the solution of the ASBL problem with instantaneous values of α and β at that time. This allows a significant computational reduction as rather than having to solve for a slowly-varying time-dependent eigenvalue $c(t)$, only the steady eigenvalue problem needs to be solved to be able to determine the unsteady solution. The steady (parallel) problem was solved for a range of values of α and β in Deguchi & Hall (2014b).

3.5 *The roll–streak flow exiting the production layer*

The roll-streak flow exiting the production layer for ASBL flow is given by (3.4). Using the transformation above and the production-layer scalings (3.9), for the Rayleigh problem we see that the roll-streak flow exiting the production layer is given by

$$u \to -A_0\frac{K}{Re}\mathrm{e}^{-y/\sqrt{2t}} + \frac{K}{Re}\frac{J_1}{\sqrt{2t}}\mathrm{e}^{(\omega_1-1)y/\sqrt{2t}}(\sqrt{2t}A_0)^{(1-\omega_1)}\cos(2K\beta_0 z) + \ldots, \qquad (3.15)$$

$$v \to \frac{K}{Re}\frac{K_1}{\sqrt{2t}}\mathrm{e}^{\omega_1 y/\sqrt{2t}}(\sqrt{2t}A_0)^{-\omega_1}\cos(2K\beta_0 z) + \ldots, \qquad (3.16)$$

where J_1, K_1 and ω_1 are functions of the instantaneous effective spanwise wavenumber β and are therefore updated at each time step. From (3.4), for growth in ASBL flow the local spanwise wavenumber must satisfy $\omega_1 - 1 > 0$, or equivalently, $\beta < 1/\sqrt{2}$ at each time step. Therefore for a given β_0, the length of time for which growth occurs in the Rayleigh problem is specified by $\beta_0\sqrt{2t} < 1/\sqrt{2}$. Hence, the free-stream coherent structures only produce an exponentially growing streak for a finite time. We also note that as with the ASBL problem, above the production layer the wave, roll and streak all decay and the flow returns to its free-stream value given by (3.12a), as with no forcing the self-sustaining mechanism breaks down away from the critical layer that produces the Reynolds stresses.

Finally we now see that if we had taken the velocity at the plate to be $(U_1,0,0)$ in §2 rather than $(-U_1,0,0)$ then we would change the sign of the streamwise velocity in (3.12b). Although the physics of the problem would be unchanged, we would not then be able to reduce exactly to the ASBL problem as the coefficient of $\mathrm{e}^{-y/\sqrt{2t}}$ in (3.15) would have a different sign. Thus we would not have been able to use the parameters obtained in the numerical results of Deguchi & Hall (2014b) as the boundary conditions would be slightly different.

4. The adjustment layer problem

We now turn our attention to what happens beneath the production layer as the disturbance produced by the nonlinear interaction in the production layer interacts with the mean flow. For the ASBL problem this is relatively simple: the streak grows exponentially all the way down to the unperturbed boundary layer, where it is ultimately reduced to zero to satisfy the wall conditions.

For the Rayleigh problem, we find that the solution is much more complicated and takes on a structure related to that found for spatially growing flow by Deguchi & Hall (2015). This is because beneath the production layer the unsteady effects, which could be forced to act in a quasi-steady manner in the production layer, come back into play. This leads to a rich asymptotic structure with two adjustment

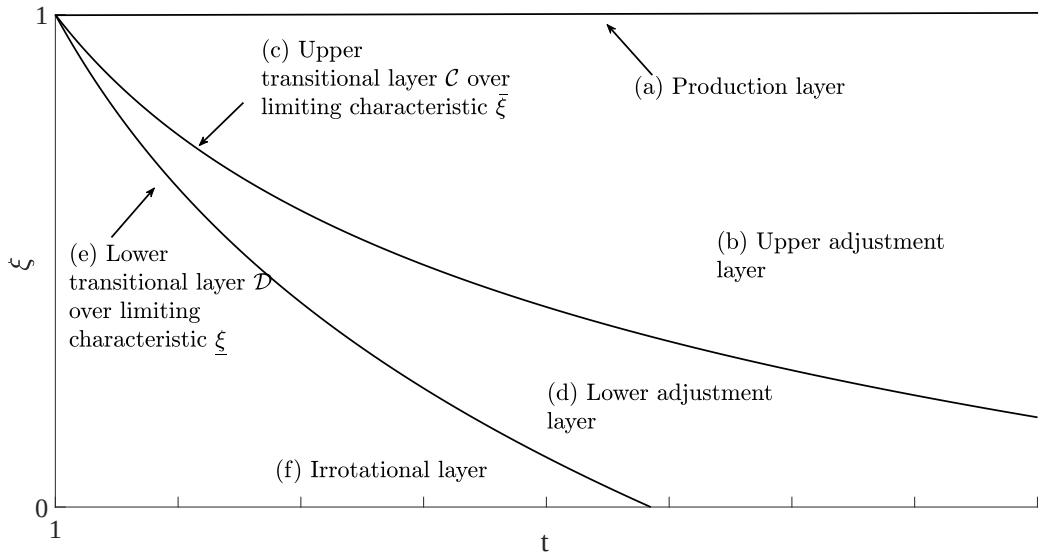

FIG. 1: The structure beneath the production layer for the unsteady problem showing the diffusion fronts, over which the WKB phase changes. Characteristics emanate from the initial point of forcing $(t,\xi) = (1,1)$.

layers and an irrotational layer separated by diffusion fronts which arise when different WKB phase solutions become dominant; see figure 1. From the three layers we can form a composite solution by matching the solution across the diffusion fronts.

We first derive the boundary-region equations, valid from the wall to the production layer, and then solve them using the WKB method. We find that the forcing from the solution exiting the production layer (region a in figure 1) dominates in an upper adjustment layer (region b) above a diffusion front $\mathscr{C}$ (region c) which arises due to a singularity from the onset of production-layer forcing. Below this curve a different WKB phase dominates in a lower adjustment layer (region d). The solution then becomes singular leading to a second diffusion front $\mathscr{D}$ (region e), below which the flow is irrotational (region f).

4.1 *The boundary-region equations*

We first find the equations describing the interaction between the production-layer solution and the basic flow and which are to be solved between the wall and the production layer. We decompose the flow field (u,v,w) into its basic flow, vortex and wave components to analyse how the disturbances exiting the production layer interact with the mean flow. The vortex component of u is called the streak flow (subscript s), and the vortex components of v and w are called the roll flow (subscript r). So if $\boldsymbol{u}_b = (u_b(t,y),0,0)$ is the basic flow in the unperturbed boundary layer, then the flow is disturbed by the

production layer forcing as

$$(u,v,w) = [u_b + u_s\cos(2K\beta_0 z), Re^{-1}v_r\cos(2K\beta_0 z), Re^{-1}w_r\sin(2K\beta_0 z)], \tag{4.1}$$

$$p = Re^{-2}p_r\cos(2K\beta_0 z). \tag{4.2}$$

We note that the spanwise wavenumber of the perturbation is taken to be β_0 to allow matching with the solution exiting the production layer (3.15)–(3.16).
We then find that the linearized boundary-region equations for the disturbance are

$$\frac{\partial}{\partial t}\begin{bmatrix} u_s \\ v_r \\ w_r \end{bmatrix} + v_r\frac{\partial}{\partial y}\begin{bmatrix} u_b \\ 0 \\ 0 \end{bmatrix} = \begin{bmatrix} 0 \\ -\partial p_r/\partial y \\ 2K\beta_0 p_r \end{bmatrix} + \left(\frac{\partial^2}{\partial y^2} - 4K^2\beta_0^2\right)\begin{bmatrix} u_s \\ v_r \\ w_r \end{bmatrix}, \tag{4.3}$$

$$\frac{\partial v_r}{\partial y} + 2K\beta_0 w_r = 0. \tag{4.4}$$

These equations are parabolic in t, and can therefore be solved by integrating in y over the region from the wall to the production layer then marching forwards subject to boundary conditions at the wall and the production layer and an initial velocity imposed at some initial value of t. Without loss of generality, it is assumed that the production-layer forcing begins at $t = 1$. We also note that the wavenumbers are dependent on t and so the problem must be solved with instantaneous values of the wavenumbers.

Considering the production-layer scalings (3.8), we now introduce a scaled variable $\xi = y/K\sqrt{2t}$ and seek a solution where $\xi = O(1)$. To enable matching with the solution exiting the production layer (3.15)–(3.16), we also adopt the production-layer scalings (3.9) for the roll-streak flow so that

$$(u_s, v_r, w_r, p_r) = (KRe^{-1}U_s, KV_r, KW_r, K^2P_r). \tag{4.5}$$

Then, the basic flow (2.5) becomes $u_b \approx A_0 KRe^{-1}\xi^{-1}\mathrm{e}^{-K^2(\xi^2-1)/2}$, so that the equation for u_s in (4.3) becomes

$$K^{-2}\left[K^{-2}\partial_\xi^2 + \xi\,\partial_\xi - 2t\left(\partial_t + 4K^2\beta_0^2\right)\right]U_s - A_0\sqrt{2t}V_r\mathrm{e}^{-K^2(\xi^2-1)/2} = 0. \tag{4.6}$$

The second equation for the roll–streak field can be found by eliminating the pressure p_r and spanwise disturbance velocity w_r from (4.3) and (4.4) to give

$$\left[K^{-2}\partial_\xi^2 + \xi\,\partial_\xi - 2t\left(\partial_t + 4K^2\beta_0^2\right)\right]\mathscr{V}_r = 0, \tag{4.7}$$

where

$$\mathscr{V}_r = [K^{-2}\partial_\xi^2 - 2t(4K^2\beta_0^2)]\,[V_r(2t)^{-1/2}]. \tag{4.8}$$

The equations (4.6)–(4.7) are solved subject to the boundary conditions

$$u \to -A_0\frac{K}{Re}\mathrm{e}^{-K^2(\xi-1)} + \frac{K}{Re}\frac{J_1}{\sqrt{2t}}\mathrm{e}^{(\omega_1-1)K^2(\xi-1)}(A_0\sqrt{2t})^{(1-\omega_1)}\cos(2K\beta_0 z) + \ldots, \tag{4.9}$$

$$v \to \frac{K}{Re}\frac{K_1}{\sqrt{2t}}\mathrm{e}^{\omega_1 K^2(\xi-1)}(A_0\sqrt{2t})^{-\omega_1}\cos(2K\beta_0 z) + \ldots. \tag{4.10}$$

as $\xi \to \infty$. The roll-flow equation (4.7) suggests that we use the WKB method to find $\mathscr{V}_r$; this solution can then be used to find V_r and U_s from (4.8) and (4.6) respectively. W_r can be then be found from the continuity equation (4.4).

4.2 *The WKB solution in the upper adjustment layer*

We now find the solution in the upper adjustment layer, region (b) in figure 1. We seek a WKB solution for $\mathscr{V}_r$ in the form

$$\mathscr{V}_r = K^2 \mathscr{V}(t,\xi,K)\mathrm{e}^{K^2\theta(t,\xi)}, \tag{4.11}$$

with $\mathscr{V}$ being the amplitude and θ being the phase in the usual notation. Substitution into the roll-flow equation (4.7) yields

$$\left[\theta_{\xi\xi}+\xi\,\theta_\xi-2t\left(\theta_t+4\beta_0^2\right)\right]\mathscr{V}+\left[K^{-4}\mathscr{V}_{\xi\xi}+K^{-2}\left(2\mathscr{V}_\xi\theta_\xi+\xi\,\mathscr{V}_\xi+\mathscr{V}\;\theta_{\xi\xi}-2t\mathscr{V}_t\right)\right]=0. \tag{4.12}$$

So at high Reynolds numbers, i.e. as $K\to\infty$, the leading order terms give the eikonal equation for the phase,

$$\theta_{\xi\xi}+\xi\,\theta_\xi-2t\left(\theta_t+4\beta_0^2\right)=0, \tag{4.13}$$

whilst at the next order the terms of order K^{-2} give an equation for the amplitude.

The forcing from the production layer initially diffuses into the adjustment layer through the phase function θ, therefore we initially consider the eikonal equation (4.13). This is a nonlinear PDE and can be solved using Charpit's method of characteristics. Defining $\hat{p}=\theta_t$ and $\hat{q}=\theta_\xi$, we seek a solution to $F(\hat{p},\hat{q},\theta,t,\xi)=0$. The Charpit equations for the eikonal equation (4.13) are

$$\frac{\mathrm{d}t}{2t}=\frac{\mathrm{d}\xi}{-(2\hat{q}+\xi)}=\frac{\mathrm{d}\hat{p}}{-(2\hat{p}+8\beta_0^2)}=\frac{\mathrm{d}\hat{q}}{\hat{q}}=\frac{\mathrm{d}\theta}{2\hat{p}-\hat{q}(2\hat{q}+\xi)}=\mathrm{d}\zeta, \tag{4.14}$$

subject to the initial Cauchy data

$$\zeta=0,\ \theta_0(s)=\hat{p}_0(s)=0,\ \hat{q}_0(s)=\omega_1(s),\ \mathscr{V}=\mathscr{V}_0(s)\text{ on }t_0(s)=s,\ \xi_0(s)=1\text{ for }s\geqslant 1, \quad (4.15a-d)$$

where s is the parametrization of the initial data, ζ is the parametrization of the characteristics and

$$\mathscr{V}_0(s)=K_1(2t)^{-1}(A_0\sqrt{2t})^{-\omega_1}[\omega_1^2-2t(4\beta_0^2)] \tag{4.16}$$

from (4.8) and (4.10). We note that $F_{\hat{p}}t_0'-F_{\hat{q}}\xi_0'\neq 0$ (where prime represents derivative) and therefore the initial data is never tangent to the solution surface; that is to say, the integrability condition is satisfied and thus the characteristics will not cross away from $\zeta=0$.

Solving the Charpit equations (4.14) yields the solution

$$t=s\mathrm{e}^{2\zeta},\quad \hat{q}=\omega_1(s)\mathrm{e}^{\zeta},\quad \hat{p}=4\beta_0^2[\mathrm{e}^{-2\zeta}-1],\quad \xi=[1+\omega_1(s)]\mathrm{e}^{-\zeta}-\omega_1(s)\mathrm{e}^{\zeta},$$

$$\theta=\left[\frac{1-\mathrm{e}^{2\zeta}}{2}\right][2s(4\beta_0^2)+\omega_1^2(s)],\quad \frac{\partial^2\theta}{\partial\xi^2}=\frac{-\mathrm{e}^{2\zeta}}{\frac{1+\omega_1(s)}{\omega_1(s)}+\mathrm{e}^{2\zeta}},\quad \mathscr{V}=\mathscr{V}_0(s)\sqrt{\frac{B(s)+1}{B(s)+\mathrm{e}^{2\zeta}}}, \quad (4.17a-g)$$

where $B(s)=(1+\omega_1(s))/\omega_1(s)$. For each value of s we can find an explicit solution for $\theta(t,\xi)$.

This solution is valid for $t>1$ where the production layer forcing begins. The characteristic emanating from that point separates what we shall define as the upper adjustment layer from the rest of the flow beneath the production layer. The limiting characteristic is at $s=1$ and is given by

$$\bar{\xi}(t)=[1+\omega_1(1)]t^{-1/2}-\omega_1(1)\sqrt{t}; \tag{4.18}$$

the corresponding amplitude on this characteristic is given by

$$\mathscr{V}=\bar{\mathscr{V}}(t)=\mathscr{V}_0(1)\sqrt{(B(1)+1)(B(1)+t)^{-1}}=\mathscr{V}^+. \tag{4.19}$$

To continue the solution below the upper adjustment layer, we stipulate that all characteristics must now pass through the singular point of initial forcing $(t,\xi)=(1,1)$.

4.3 *The WKB solution in the lower adjustment layer*

We seek a solution in the lower adjustment layer (region d in figure 1) to the Charpit equations (4.14) subject to the initial data

$$\zeta = 0, \quad \hat{p}_0(s) = 0, \quad \theta_0(s) = 0, \quad \hat{q}_0(s) = \hat{q}_0(s) \quad \text{at} \quad t = 1,\ \xi = 1 \quad \text{for} \quad s \geqslant \omega_1(1). \quad (4.20a-d)$$

We can think of this as the initial data, which was previously parametrised along t, degenerating into a point in the (t,ξ) plane. We therefore continue the initial data curve in θ_ξ as this carries the information about how the phase changes along each characteristic curve in the lower adjustment layer.

We again solve the Charpit equations to give

$$\mathrm{e}^{\zeta} = \sqrt{t}, \quad \hat{q} = q_0(s)\sqrt{t}, \quad \hat{p} = 4\beta_0^2[t^{-1}-1], \quad \xi = \frac{1+q_0(s)}{\sqrt{t}} - q_0(s)\sqrt{t},$$

$$\theta = [q_0(s)^2 + 2(4\beta_0^2)]\left[\frac{1-t}{2}\right], \frac{\partial^2\theta}{\partial\xi^2} = \frac{-t}{t-1}, \quad \mathscr{V} = g(s)\frac{1}{\sqrt{\mathrm{e}^{2\zeta}-1}}, \quad (4.21a-g)$$

where $g(s)$ is some as yet unknown function as we cannot prescribe initial data on $\mathscr{V}$ at the singular point. We note that $q_0(s)$ can be eliminated to give an explicit solution for $\theta(t,\xi)$.

4.4 *The WKB solution in the first transitional layer*

The solutions for $\theta_{\xi\xi}$ in (4.17) and (4.21) do not match at the limiting characteristic $\bar{\xi}$ given by (4.18). Therefore we introduce a diffusion front $\mathscr{C}$ to smooth out this discontinuity, shown by region (c) in figure 1. Mathematically, this diffusion front arises as the two different WKB phases of the roll-flow equation (4.7) meet. The thickness of the transitional layer is fixed by observing that because only $\theta_{\xi\xi}$ is discontinuous across the layer, upon passing through the layer the exponential dependence must change by a factor

$$\exp[K^2(\xi-\bar{\xi})^2(\bar{\theta}^+_{\xi\xi} - \bar{\theta}^-_{\xi\xi})/2] = \exp[K^2(\xi-\bar{\xi})^2 J/2], \quad (4.22)$$

where plus and minus represent the upper and lower adjustment layer solutions, and the overbar denotes a quantity evaluated on $\mathscr{C}$, so ξ is thus $O(K^{-1})$. Thus in the diffusion front we look for a WKB solution of the form

$$\mathscr{V}_r = K^2\mathscr{V}^C(t,\phi)\mathrm{e}^{K^2\theta^C(t,\phi,K)}, \quad \phi = K(\xi-\bar{\xi})/\Delta, \quad \Delta = \sqrt{2/J}, \quad (4.23a-c)$$

where superscript C represents the Taylor-series expansion truncated at $O(\xi^2)$ around the limiting characteristic $\xi = \bar{\xi}$. In this layer the higher order terms of the roll-flow equation (4.12), which were previously ignored, are reintroduced to smooth out the discontinuity.

After some manipulation (for further details see Deguchi & Hall 2015), we find that

$$\mathscr{V}^C = \bar{\mathscr{V}}(t)(\mathrm{erf}(\phi)+1)/2, \quad (4.24)$$

where $\bar{\mathscr{V}}(t)$ is given in (4.19).

Then we can find the full solution in the lower adjustment layer; by matching with the solution in the lower adjustment layer (4.21g), we obtain

$$g(s) = -\mathscr{V}_0(1)/[K\sqrt{2\pi}(s-\omega_1(1))]. \quad (4.25)$$

Thus we find that in the lower adjustment layer the amplitude is given by

$$\mathscr{V} = \frac{\mathscr{V}_0(1)\sqrt{t-1}}{K\sqrt{2\pi}[\xi\sqrt{t}-1+\omega_1(1)(t-1)]} = \mathscr{V}^-, \tag{4.26}$$

with $\mathscr{V}_0(1)$ given by (4.16). So in particular, we see that the amplitude falls by a factor of K^{-1} when crossing the diffusion front $\mathscr{C}$.

4.5 *The roll–streak flow in the upper and lower adjustment layers*

The roll and streak flow can now be found from (4.7) and (4.6) respectively. We obtain

$$V_r = \frac{\sqrt{2t}\mathscr{V}\mathrm{e}^{K^2\theta}}{\theta_\xi^2 - 2t(4\beta_0^2)}, \quad U_s = -\frac{A_0\xi^{-1}\sqrt{2t}}{2\theta_\xi}\mathrm{e}^{-\frac{K^2}{2}(\xi^2-1)}V_r, \tag{4.27a,b}$$

where in the upper adjustment layer θ and $\mathscr{V}$ are as given in (4.17), whereas for the lower adjustment layer θ is as given in (4.21) and $\mathscr{V}$ is as given in (4.26).

We see that this solution becomes singular when $s = \sqrt{2}(2\beta_0)$. This corresponds to a second limiting characteristic

$$\xi = \frac{1+2\sqrt{2}\beta_0}{\sqrt{t}} - 2\sqrt{2}\beta_0\sqrt{t} \equiv \underline{\xi}(t). \tag{4.28}$$

4.6 *The WKB solution in the second transitional layer*

To smooth out the singularity we introduce a second diffusion front $\mathscr{D}$ which separates the upper and lower adjustment layers from the rest of the flow (region e in figure 1). Mathematically this curve arises because the homogeneous terms of the WKB solution have become as large as the inhomogeneous terms. Again the thickness of the layer is defined by insisting that the second-derivative amplitude terms in (4.7) are as large as the phase terms; once again this requires that the layer is of thickness $O(K^{-1})$. Thus in the diffusion front we seek a WKB solution of the form

$$V_r = V^D(t,\varphi)\mathrm{e}^{K^2\theta^D(t,\varphi,K)}; \quad \varphi = K(\xi-\underline{\xi})/\delta(t), \quad \delta(t) = \sqrt{-2/\theta^-_{\xi\xi}}, \tag{4.29$a-c$}$$

where θ_D is the Taylor expansion truncated at $O(\xi^2)$ of the phase (4.21) in the lower adjustment layer. By considering the limiting form of V^D, we can obtain a match with the lower adjustment layer solution.

We find that the amplitude of the roll in $\mathscr{D}$ is given by

$$V^D = V^i\mathrm{e}^{\varphi^2}\left[\frac{\mathrm{erf}(\varphi)-1}{2}\right], \tag{4.30}$$

where

$$V^i(t) = -\frac{\mathscr{V}_0(1)}{4\beta_0[2\sqrt{2t}\beta_0 - \omega_1(1)\sqrt{t}]}. \tag{4.31}$$

So in particular, we see that the amplitude is once again $O(1)$; that is, the amplitude grows by a factor K across the second diffusion layer.

4.7 *The WKB solution in the irrotational layer*

Beneath $\mathscr{D}$ the flow is irrotational because the forcing from the production layer cannot reach this part of the flow. By again using the roll–streak equations (4.6) and (4.7), we find that the streak and roll flow in this irrotational layer are given by

$$V_r = -V^i(t)\mathrm{e}^{K^2\theta^i(t,\xi)}, \quad U_s = -\frac{\sqrt{2t}A_0\mathrm{e}^{-\frac{K^2}{2}(\xi^2-1)}V_r}{2\xi\theta^i_\xi}, \tag{4.32a,b}$$

where

$$\theta^i(t,\xi) = 2(4\beta_0^2)(1-t) + 2\sqrt{2\tau}\beta_0(\xi-\underline{\xi}). \tag{4.33}$$

4.8 *The full composite roll–streak solution*

We now combine the solutions from each of the three layers, along with the limiting solutions from each diffusion front, to produce a composite solution for the phase which is valid for the entire flow beneath the production layer. We define the composite solution so that under taking the logarithm it becomes (inner solution) + (outer solution) - (common part).

Firstly, the WKB phase solution θ is continuous everywhere beneath the production layer and is defined as

$$\theta = \begin{cases} \theta^+ \text{ from (4.17)} & \xi \geqslant \bar{\xi}, \\ \theta^- \text{ from (4.21)} & \bar{\xi} > \xi \geqslant \underline{\xi}, \\ \theta^i \text{ from (4.33)} & \xi < \underline{\xi}. \end{cases} \tag{4.34}$$

Then, to smooth out the singularities of the amplitude when crossing the lower adjustment layer, we define a composite solution for the roll flow in terms of the limiting forms as

$$V_r = \begin{cases} \dfrac{\mathscr{V}^C}{\mathscr{V}^C_\infty}\dfrac{\mathscr{V}^D}{\mathscr{V}^D_\infty}\dfrac{\sqrt{2t}\mathscr{V}^+\mathrm{e}^{K^2\theta}}{\theta_\xi^2 - 2t(4\beta_0^2)} \text{ from (4.19)} & \xi \geqslant \bar{\xi}, \\ \dfrac{\mathscr{V}^C}{\mathscr{V}^C_{-\infty}}\dfrac{\mathscr{V}^D}{\mathscr{V}^D_\infty}\dfrac{\sqrt{2t}\mathscr{V}^-\mathrm{e}^{K^2\theta}}{\theta_\xi^2 - 2t(4\beta_0^2)} \text{ from (4.26)} & \bar{\xi} > \xi \geqslant \underline{\xi}, \\ \dfrac{-\mathscr{V}^C}{\mathscr{V}^C_{-\infty}}\dfrac{\mathscr{V}^D}{\mathscr{V}^D_{-\infty}}V_i(t)\mathrm{e}^{K^2\theta^i(t,\xi)} \text{ from (4.31)} & \xi < \underline{\xi}. \end{cases} \tag{4.35}$$

The limiting forms $\mathscr{V}^C_\infty$, $\mathscr{V}^C_{-\infty}$, $\mathscr{V}^D_\infty$ and $\mathscr{V}^C_{-\infty}$ are the limits as $\phi \to \pm\infty$ and $\varphi \to \pm\infty$ of (4.24) and (4.30) respectively.

The roll flow then completely defines the streak flow as

$$U_s = -\frac{A_0\xi^{-1}\sqrt{2t}}{2\theta_\xi}\mathrm{e}^{-\frac{K^2}{2}(\xi^2-1)}V_r, \tag{4.36}$$

where θ is defined in each layer by (4.34). Then W_r can be found from the continuity equation (4.4).

4.9 *The location of the streak maximum*

The streak flow in each layer, given by (4.36) for each θ as in (4.34), has exponential dependence with argument $K^2(\theta - \xi^2/2 - 1/2)$. This exponential dependence dominates the size of the streak. Therefore,

defining $M = M(t,\xi) = K^2(\theta - \xi^2/2 - 1/2)$, the streak maximum occurs where $M_t = M_\xi = 0$. Thus using the eikonal equation (4.13), we find that the streak maximum occurs where

$$\xi = 2\beta_0\sqrt{t}; \quad 2\beta_0 = \frac{1}{2t-1}. \tag{4.37a,b}$$

Thus, the maximum of the streak occurs in the lower adjustment layer, i.e. $\bar{\xi} > \xi_M \geqslant \xi$. This means that the maximum occurs well after the onset of forcing, and far away from the wall at $\bar{\xi} = 0$. Hence, the streak structure is more dominant in the lower adjustment layer where $\xi = O(1)$ than in the unperturbed main boundary layer where $\xi = O(K^{-1})$. Surprisingly, this is the layer where the WKB amplitude is a minimum. This is because the dominant forcing from the production layer occurs through the phase.

5. Numerical results

We now present numerical solutions of the boundary-region equations (4.3)–(4.4) and compare them against the composite solution (4.35)–(4.36) found in §4. To calculate the numerical solution of the boundary-region equations (4.3)–(4.4), we march the equations forward in time from an initial condition, subject to boundary conditions at the wall and at the production layer. At each time step we evaluate the boundary conditions (3.15)–(3.16) using the instantaneous value of $K_1(\alpha,\beta)$ given by the solution of the numerical eigenvalue problem for ASBL flow, (3.2)–(3.3), solved for a range of (α,β) in Deguchi & Hall (2014b). Here we recall α and β are the instantaneous wavenumbers $\alpha = \alpha_0\sqrt{2t}$, $\beta = \beta_0\sqrt{2t}$. We solve for values of β lying between the left and right saddle nodes of the numerical eigenvalue solutions from Deguchi & Hall (2014b) for the production layer problem; taking the left saddle node to correspond to $t = 1$, this then fixes a time interval on which to compute the solution and thus also fixes the range of spanwise wavenumbers β. We find that there is good agreement between the asymptotic results and the numerical solutions.

The boundary-region equations (4.3) are parabolic and therefore, given values of the Reynolds number and the spanwise wavenumber, can be solved numerically by marching forwards in time subject to initial forcing from the production layer.

Following Hall (1983) we first rearrange the boundary-region equations (4.3)–(4.4) and eliminate the pressure and spanwise velocity disturbances to give a fourth order equation for the roll flow v_r and a second order equation for the streak flow u_s. Then, after writing the equations in terms of the similarity variable $\eta = y/\sqrt{2t}$, the equations are discretized in η using a second-order-accurate central finite-difference scheme.

We then use a second-order-accurate Crank-Nicholson scheme to march the equations forward in time. We use a step size of $h = 10^{-3}$ in the t direction, and a grid of 2000 points in the η direction. We apply an initial condition $u_s = v_r = 0$ at $t = 1$ for all η. At the wall we apply no-slip and impenetrability, so that $u_s = v_r = \partial v_r/\partial y = 0$ at $\eta = 0$. At the production layer, corresponding to $\eta = K$, we apply the boundary conditions (3.15)–(3.16) and $\partial v_r/\partial y = 0$.

In figure 2 we present results for the numerical solution for $Re = 10^4$, 10^7 and 10^{10}. In figures 2a, 2c and 2e we show the streak part of the numerical solution of the boundary-region equations, together with the limiting characteristics shown in figure 1. In addition we show the asymptotic prediction of the streak maximum in t and ξ given by (4.37). We see that as the Reynolds number increases the numerical results agree increasingly well with the asymptotic results; this is shown by the observed maximum of the numerical solution falling increasingly close to the predicted location of the maximum of M in t

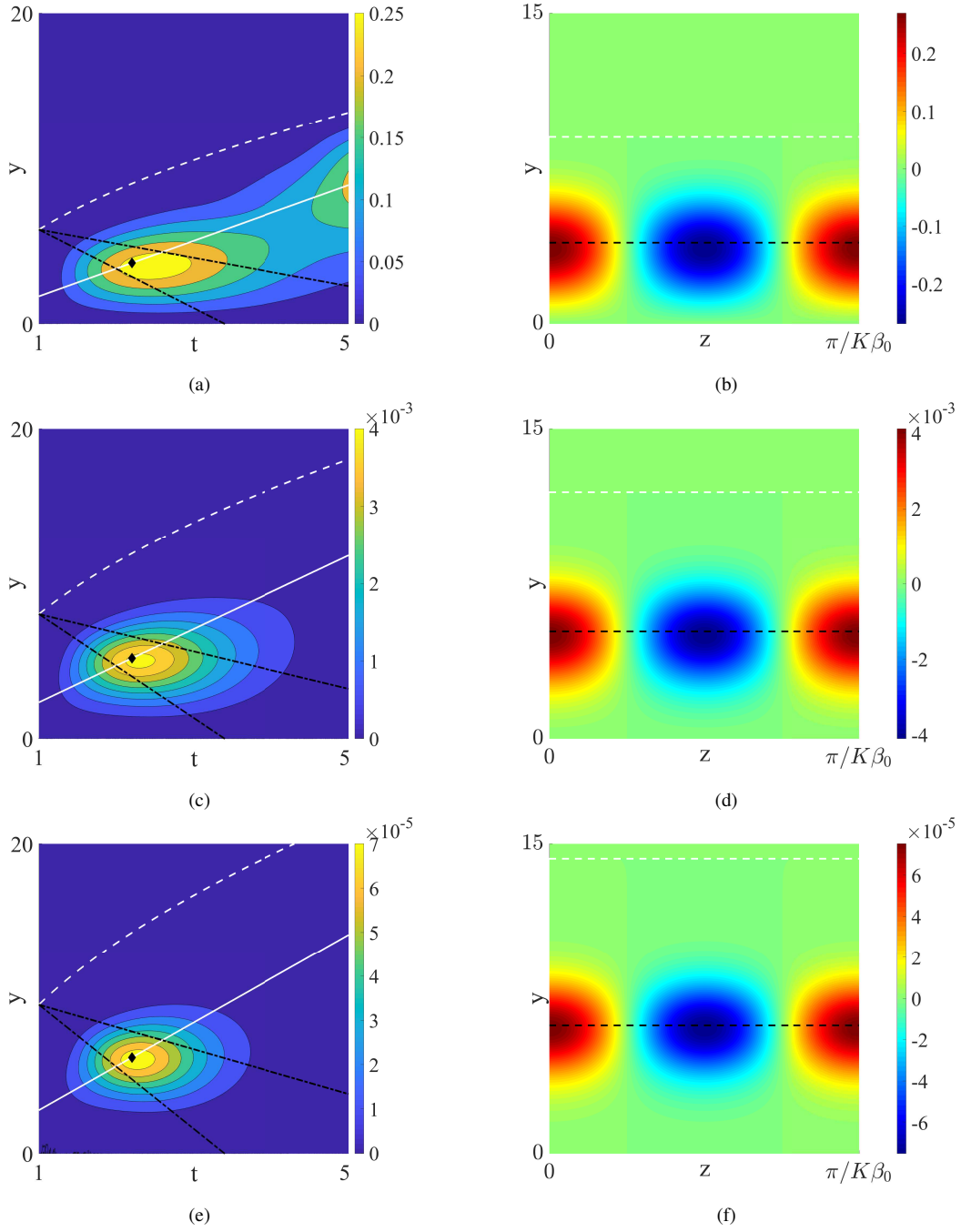

FIG. 2: The numerical solution for $Re = 10^4$ (a, b), 10^7 (c, d) and 10^{10} (e, f). (a, c, e): The streak part of the solution $-u_s$. The black dashed lines are the upper and lower limiting characteristics $\bar{\xi}$ and $\underline{\xi}$ from (4.18) and (4.28) respectively. The white line corresponds to the predicted location of the maximum of M in t and ξ from (4.37), with the corresponding time marked by a black diamond (⧫). The white dashed line is $\xi = 1$ (at the production layer). (b, d, f): The disturbance streamwise velocity $-u_s \cos(2K\beta_0 z)$ at the predicted time of the streak maximum, $t \approx 2.21$. The black dashed line is the predicted location of the maximum of M in ξ at this time. The white dashed line is $\xi = 1$.

and ξ, marked by a black diamond (♦). The numerical solution also improves over long times as the Reynolds number increases; for $Re = 10^4$ there is some error at larger values of t, however here the expansion parameter K used is only approximately 4. However in all cases the numerical solution has captured the predicted overall flow structure; that is, $O(Re^{-1})$ interactions taking place in the production layer produce a large amplitude streak appearing in the boundary layer, albeit for a finite time.

In figures 2b, 2d and 2f we show the disturbance streamwise velocity in the $y-z$ plane at the predicted time for the streak maximum to occur from (4.37). We see that the location of the predicted streak maximum agrees increasingly well with the numerical results as the Reynolds number is increased. We also clearly see the streak, having grown away from the production layer, obtaining its maximum well away from the production layer where it was generated.

6. Discussion

We have shown that free-stream coherent structures can exist in unsteady Rayleigh boundary-layer flow. The structures were mathematically similar to those derived in Deguchi & Hall (2015), with the flow unsteadiness replacing non-parallel effects. An $O(Re^{-1})$ nonlinear interaction in a layer situated just below the free-stream, where disturbances were convected with almost free-stream speed, produced a disturbance involving rolls, waves and streaks. The streak part of this disturbance interacted with the basic flow in the main part of the boundary layer and continued to grow through the 'lift-up' mechanism, adjusting to the non-parallel nature of the basic flow via continuation through two transitional layers where discontinuities were smoothed to produce a composite solution. The streak maximum was predicted to be in the lower of the two adjustment layers. The asymptotically-reduced boundary-region equations were then solved numerically via a Crank-Nicholson time-marching scheme. The numerical results were found to be in increasingly good agreement with the predicted asymptotic results as the Reynolds number was increased. In particular, as the Reynolds number was increased, the streak maximum in the numerical solution appeared earlier, in better agreement with the asymptotic prediction.

Unsteady flows are ubiquitous in nature and have many applications in engineering and science. The unsteadiness is mainly classed as non-periodic, for example the sudden opening and closing of valves in a flow through a pipe system or periodic, for example a turbine blade rotating through water. The Rayleigh problem studied here is non-periodic, but the laminar flow allows a similarity solution. Experimental results for transition to turbulence in non-periodic unsteady flows by Mathur et al. (2018) have shown that if the flow is persistently accelerated the critical Reynolds number associated with transition increases. In addition, for periodic unsteadiness flows or flows where the unsteadiness is changing, for example by acceleration, the flow history is important: the way in which instantaneous flow behaves is based on past history. In light of those results variations on the Rayleigh problem in which the quasi-steady approximation is not valid would provide interesting areas of further study. These include an oscillating flat plate (Stokes' second problem), and a flat plate accelerated uniformly from rest. The first of these has an analytic solution for the basic flow which approaches its free-stream value through an exponentially small correction so could be particularly interesting to study in light of the results above. However since it is not exponential throughout the main boundary layer the interaction of a streak disturbance with the basic flow could be very different and may not support growth.

We also note here that we have not solved the unsteady production layer problem; such solutions, if they exist, could be used to analyse the small-time development of the problem studied here. We have not gone into detail here on the solution at the immediate point of forcing, when a singularity occurs. Here, the characteristics described in §4 pile up and a shock in the solution occurs. However, since the maximum of the streak disturbance occurs in the adjustment layer well away from the initial

forcing at $t = 1$, it is anticipated that nothing new would be learnt about the solution by examining this region. Nevertheless, for a periodic or accelerating unsteadiness where, as discussed above, flow history is important, the shock at the initial point of forcing could have great implications at later times.

Laminar Rayleigh flow is often used to show how vorticity spreads in a boundary layer. The basic flow and the vorticity both satisfy the heat equation for the conduction of heat on a semi-infinite rod. In the context of fluid flow, the wall becomes a plane source of vorticity and the Rayleigh problem shows how fluid momentum is diffused away from the plate, with the region affected by viscosity (i.e. the boundary layer) growing in time; we earlier showed the width of the boundary layer to be $\sim \sqrt{\nu t}$. In addition, one can show that the shear stress at the wall decays as $t^{-1/2}$. With the free-stream coherent structures we now have high levels of vorticity entering the boundary layer from the free-stream. It would be interesting to examine the interaction of the basic underlying vorticity field with the vorticity originating in the production layer; this could be done asymptotically in a similar manner to the problem described above.

The flat plate studied in this problem was infinitely long and therefore the free-stream coherent structures found were independent of the point x from the flow was viewed. An interesting problem to study further would be that of a semi-infinite flat plate moving with constant unit velocity. For time $t < x$, where x is the distance measured downstream from the leading edge, Rayleigh flow is observed. However beyond that point the flow is radically different; at $t = x$ the disturbance at the leading edge begins to affect the flow and for $t \to \infty$, Blasius flow is observed. Therefore we have a remarkable situation where an x-independent, time-dependent flow can smoothly change (this is a physical requirement) into a time-independent, x-dependent flow. There are conflicting explanations as to how this occurs; Smith (1972) and Stewartson (1951) claim that it occurs through an essential singularity whereas Tokuda (1968) claims that the solution can be found without a singularity through the use of stretched variables. The question of how the free-stream coherent structures develop at this point is particularly intriguing; in particular, whether the transition point could provide any forcing to sustain the structures past the point where no growth occurs in these results.

The authors very much appreciate the constructive marks of the referees.

REFERENCES

Brown, S. N. & Stewartson, K. (1965) On similarity solutions of the boundary-layer equations with algebraic decay. *J. Fluid Mech.*, **23**(4), 673–687.

Chen, C. & Christensen, D. K. (1967) Stability of flow induced by an impulsively started rotating cylinder. *Phys. Fluids*, **10**(8), 1845–1846.

Cowley, S. (1987) 'High frequency Rayleigh instability of Stokes layers'. In Dwoyer, D. & Hussaini, M., editors, *Stability of Time Dependent and Spatially Varying Flows*, pages 261–275. Springer.

Deguchi, K. & Hall, P. (2014a) Canonical exact coherent structures embedded in high Reynolds number flows. *Philosophical Transactions of the Royal Society A: Mathematical, Physical and Engineering Sciences*, **372**(2020), 20130352.

Deguchi, K. & Hall, P. (2014b) Free-stream coherent structures in parallel boundary-layer flows. *J. Fluid Mech.*, **752**, 602–625.

Deguchi, K. & Hall, P. (2015) Free-stream coherent structures in growing boundary layers: a link to near-wall streaks. *J. Fluid Mech.*, **778**, 451–484.

Deguchi, K. & Hall, P. (2018) Free-stream coherent structures in a planar jet. *Journal of Fluid Mechanics*, **837**, 916.

Faisst, H. & Eckhardt, B. (2003) Traveling waves in pipe flow. *Phys. Rev. Lett.*, **91**(22), 224502.

Goldstein, M. & Sescu, A. (2008) Boundary-layer transition at high free-stream disturbance levels-beyond Kle-

banoff modes. *J. Fluid Mech.*, **613**, 95.

Hall, P. (1978) The linear stability of flat Stokes layers. *P. Roy. Soc. A*, **359**(1697), 151–166.

Hall, P. (1983) The linear development of Görtler vortices in growing boundary layers. *J. Fluid Mech.*, **130**, 41–58.

Hall, P. (2003) On the instability of Stokes layers at high Reynolds numbers. *J. Fluid Mech.*, **482**, 1.

Hall, P. & Parker, K. H. (1976) The stability of the decaying flow in a suddenly blocked channel. *J. Fluid Mech.*, **75**(2), 305–314.

Hall, P. & Sherwin, S. (2010) Streamwise vortices in shear flows: harbingers of transition and the skeleton of coherent structures. *J. Fluid Mech.*, **661**, 178–205.

Hall, P. & Smith, F. T. (1991) On strongly nonlinear vortex/wave interactions in boundary-layer transition. *J. Fluid Mech.*, **227**, 641–666.

Jiménez, J. (2018) Coherent structures in wall-bounded turbulence. *J. Fluid Mech.*, **842**, P1.

Kirchner, R. & Chen, C. (1970) Stability of time-dependent rotational Couette flow. Part 1. Experimental investigation. *J. Fluid Mech.*, **40**(1), 39–47.

Luchini, P. (1996) Reynolds-number-independent instability of the boundary layer over a flat surface. *Journal of Fluid Mechanics*, **327**, 101–115.

Martin, J. & Martel, C. (2012) Nonlinear streak computation using boundary region equations. *Fluid Dyn. Res.*, **44**(4), 045503.

Mathur, A., Seddighi, M. & He, S. (2018) Transition of transient channel flow with high Reynolds number ratios. *Entropy*, **20**(5).

Moss, E. (1992) 'The stability of spatially developed pipe flows impulsively started from rest'. In *Eleventh Australasian Fluid Mechanics Conference, Univ. of Tasmania, Hobart, Australia, 14-18 December 1992*, pages 703–706.

Otto, S. R. (1993) Stability of the flow around a cylinder: the spin-up problem. *IMA J. Appl. Math.*, **51**(1), 13–26.

Ricco, P., Luo, J. & Wu, X. (2011) Evolution and instability of unsteady nonlinear streaks generated by free-stream vortical disturbances. *J. Fluid Mech.*, **677**, 1.

Seminara, G. & Hall, P. (1975) Linear stability of slowly varying unsteady flows in a curved channel. *P. Roy. Soc. A*, **346**(1646), 279–303.

Sescu, A. & Afsar, M. (2018) Hampering Görtler vortices via optimal control in the framework of nonlinear boundary region equations. *J. Fluid Mech.*

Shen, S. (1961) Some considerations on the laminar stability of time-dependent basic flows. *J. Aerospace Sci*, **28**(5), 397–404.

Smith, S. H. (1972) On the impulsive flow of a viscous liquid past a semi-infinite flat plate. *SIAM. J. Appl. Math.*, **22**(2), 148–154.

Stewartson, K. (1951) On the impulsive motion of a flat plate in a viscous fluid. *Q. J. Mech. Appl. Math*, **4**(2), 182–198.

Thomas, C. (2020) The linear stability of an acceleration-skewed oscillatory Stokes layer. *J. Fluid Mech.*, **895**.

Tokuda, N. (1968) On the impulsive motion of a flat plate in a viscous fluid. *J. Fluid Mech.*, **33**(4), 657–672.

Von Kerczek, C. & Davis, S. H. (1974) Linear stability theory of oscillatory Stokes layers. *J. Fluid Mech.*, **62**(4), 753–773.

Waleffe, F. (1997) On a self-sustaining process in shear flows. *Phys. Fluids*, **9**(4), 883–900.

Waleffe, F. (2001) Exact coherent structures in channel flow. *J. Fluid Mech.*, **435**, 93–102.

Waleffe, F. (2003) Homotopy of exact coherent structures in plane shear flows. *Phys. Fluids*, **15**(6), 1517–1534.

Wang, J., Gibson, J. & Waleffe, F. (2007) Lower branch coherent states in shear flows: transition and control. *Phys. Rev. Lett.*, **98**(20), 204501.

Wedin, H. & Kerswell, R. R. (2004) Exact coherent structures in pipe flow: travelling wave solutions. *J. Fluid Mech.*, **508**, 333–371.

Wu, X. (1992) The nonlinear evolution of high-frequency resonant-triad waves in an oscillatory Stokes layer at high

Reynolds number. *J. Fluid Mech.*, **245**, 553–597.

Wu, X., Lee, S. & Cowley, S. J. (1993) On the weakly nonlinear three-dimensional instability of shear layers to pairs of oblique waves: the Stokes layer as a paradigm. *J. Fluid Mech.*, **253**, 681–721.